Physics of the Earth and Planetary Interiors 233 (2014) 24–32

Contents lists available at ScienceDirect

Physics of the Earth and Planetary Interiors

journal homepage: www.elsevier.com/locate/pepi

Sound velocities of bcc-Fe and $Fe_{0.85}Si_{0.15}$ alloy at high pressure and temperature

Jin Liu [a,*], Jung-Fu Lin [a], Ahmet Alatas [b], Wenli Bi [b,c]

[a] Department of Geological Sciences, Jackson School of Geosciences, University of Texas at Austin, Austin, TX 78712, USA
[b] Advanced Photon Source, Argonne National Laboratory, Argonne, IL 60439, USA
[c] Department of Geology, University of Illinois at Urbana-Champaign, Urbana, IL 61801, USA

ARTICLE INFO

Article history:
Received 14 February 2014
Received in revised form 28 April 2014
Accepted 7 May 2014
Available online 28 May 2014

Keywords:
Compressional wave velocity
High pressure-temperature
Light elements
Inelastic X-ray scattering

ABSTRACT

Studying the velocity–density profiles of iron and iron–silicon alloy at high pressures and temperatures is critical for understanding the Earth's core as well as the interiors of other planetary bodies. Here we have investigated the compressional wave velocity (V_P) and density (ρ) profiles of polycrystalline bcc-Fe and $Fe_{0.85}Si_{0.15}$ alloy (8 wt.% Si) using *in situ* high-energy resolution inelastic X-ray scattering (HERIX) and synchrotron X-ray diffraction spectroscopies in an externally-heated diamond anvil cell (EHDAC) up to 15 GPa and 700 K. Based on the measured velocity–density (V_P–ρ) and velocity–pressure (V_P–P) relations of bcc-Fe at simultaneous high pressure and temperature (P–T) conditions, our results show a strong V_P reduction at elevated temperatures at a constant density. Comparison of the V_P–ρ profiles between the bcc-Fe and bcc-$Fe_{0.85}Si_{0.15}$ alloy indicates that the alloying effect of additional 8 wt.% Si on the V_P–ρ relationship of bcc-Fe is predominant via a constant density decrease of approximately 0.6 g/cm^3 (7%). Compared with the literature velocity results for bcc and hcp Fe–Si alloys, the bcc-Fe and Fe–Si alloys exhibit higher V_P than their hcp phase counterparts at the given bcc–hcp transition pressures. Our results here strongly support the notion that high temperature has a strong effect on the V_P of Fe and that the V_P–ρ profile of Fe can be affected by structural and magnetic transitions. Analyses on literature elastic constants of the bcc Fe–Si alloys, as a function of P–T and Si content, show that the bcc phase displays extremely high V_P anisotropy of 16–30% and V_S splitting anisotropy of 40–90% at high temperatures, while the addition of Si further enhances the anisotropy. Due to the extremely high elastic anisotropy of the bcc Fe–Si alloy, a certain portion of the bcc Fe–Si alloy with the lattice-preferred orientation may produce V_P and V_S anisotropies to potentially account for the observed seismic anisotropy in the inner core.

1. Introduction

Earth's core is predominantly constituted of Fe, alloyed with Ni and a certain amount (approximately 10 wt.%) of elements lighter than Fe (thus named light elements) (Birch, 1952, 1964). A plethora of studies have concentrated on the identity and concentration of candidate light elements incorporated into the Earth's core from cosmochemical, geochemical, geophysical, and mineral physics perspectives (e.g., Birch, 1952, 1964; Poirier, 1994; McDonough and Sun, 1995; Zhang and Guyot, 1999; Alfè et al., 2002; Lin et al., 2002; Li and Fei, 2003; Rubie et al., 2007, 2011); though, the crystal structure and the amount of the major light element alloyed with Fe in the Earth's core remain highly debated (see Dubrovinsky and Lin (2009) for further reviews). To date, a number of plausible major light elements have been proposed, including Si, S, O, C, and H (see Poirier (1994) and Li and Fei (2003) for further details). These results indicate that the presence of approximately 10 wt.% light elements in the Earth's core is necessary to explain the density and velocity discrepancies between seismic observations and measured velocity–density profiles of pure iron (Birch, 1964). However, most of the proposed major light elements have very low solubility in Fe at ambient conditions or at limited high P–T conditions (Li and Fei, 2003; Chen et al., 2008), making it difficult to investigate the alloying effects of the light element on thermodynamic and elastic properties of iron at relevant conditions of the Earth's core. On the other hand, Si can be readily alloyed with Fe in the hexagonal closest-packed (hcp), body-centered cubic (bcc), or bcc-related structures (Machová and Kadečková, 1977; Lin et al., 2003a; Kuwayama et al., 2009;

* Corresponding author. Tel.: +1 5128148048.
E-mail address: jinliu@utexas.edu (J. Liu).

http://dx.doi.org/10.1016/j.pepi.2014.05.008
0031-9201/

Fischer et al., 2013), allowing one to study the alloying effects of a potential light element more easily.

Recent studies on the phase diagram of iron-light element alloys at relevant P–T conditions of the Earth's inner core have shown very rich information about their crystal structures, melting point depressions, elasticity, and alloying effects of light elements (see Li and Fei (2003) and Rubie et al. (2007) for further reviews). Synchrotron X-ray diffraction (XRD) experiments and theoretical calculations on the crystal structure of pure iron have shown that the hcp structure is likely to be the most stable phase at relevant P–T conditions of the Earth's inner core (Kuwayama et al., 2008; Vočadlo et al., 1999; Tateno et al., 2010; Stixrude, 2012). Furthermore, the face-centered cubic (fcc) structure of Fe has also been suggested to coexist with the hcp phase in the inner core (Mikhaylushkin et al., 2007; Côté et al., 2010; Cui et al., 2013). On the other hand, the bcc structure of Fe or its alloys, including Fe–Si and Fe–Ni alloys, may also exist in the inner core conditions (e.g., Brown and McQueen, 1986; Matsui and Anderson, 1997; Lin et al., 2002; Lin et al., 2003a; Belonoshko et al., 2003; Belonoshko et al., 2006; Belonoshko et al., 2008a,b; Belonoshko et al., 2009; Belonoshko et al., 2011; Vočadlo et al., 2003, 2008; Hirao et al., 2004; Dubrovinsky et al., 2007; Sata et al., 2008; Kuwayama et al., 2009; Asanuma et al., 2010; Luo et al., 2010; Zhang and Oganov, 2010; Persson et al., 2011; Fischer et al., 2013). Recent experimental and theoretical results revealed that addition of Si light element and/or Ni in Fe can stabilize the bcc phase at higher P–T conditions relevant to the inner core as a result of the combined effects of high-temperature and addition of light elements in Fe (Lin et al., 2002; Dubrovinsky et al., 2007; Vočadlo et al. 2008; Côté et al., 2008; Kuwayama et al., 2009). It has also been argued that the complex structure and P-wave anisotropy of the inner core can be better explained by the presence of the textured bcc phase with extremely high elastic anisotropy, instead of a single phase of hcp-Fe (Belonoshko et al., 2008a; Mattesini et al., 2010, 2013; Geballe et al., 2013). On the other hand, the anisotropy of hcp-Fe is reported to decrease with increasing pressure and/or temperature (e.g., Stixrude and Cohen, 1995; Steinle-Neumann et al., 2001; Vočadlo et al., 2009; Sha and Cohen, 2010). Several previous studies have indicated that the anisotropy of hcp-iron can be so small (~1%) or insignificant under the Earth's core conditions such that it may not be sufficient to explain the seismic V_P and V_S anisotropies of the inner core (Belonoshko et al., 2003; Sha and Cohen, 2010). Therefore, knowledge about the sound velocity of the bcc-Fe and Fe–Si alloys at high P–T conditions can provide further new insights into our understanding of the geophysics and geochemistry of the Earth's core as well as the interiors of other planetary bodies (Sohl and Schubert, 2007).

A number of experimental high-pressure techniques, including ultrasonic interferometry, nuclear resonant inelastic X-ray scattering (NRIXS), high-energy resolution inelastic X-ray scattering (HERIX), impulsive stimulated light scattering (ISLS), and shock compression, have been used to measure the compressional wave velocity (V_P) of the hcp-Fe at high pressures (e.g., Mao 1998, 2001; Fiquet et al., 2001; Crowhurst et al. 2004; Nguyen and Holmes, 2004). Sound velocities of Fe alloys (e.g., Fe–Ni, Fe–O–S, Fe–Ni–Si, Fe–H) and Fe-bearing compounds (e.g., Fe_3C, Fe_3S, FeO, FeSi) have also been systematically investigated (e.g., Lin et al., 2003b; Fiquet et al., 2004; Mao et al., 2004; Badro et al., 2007; Kantor et al., 2007; Whitaker et al. 2009; Antonangeli et al., 2010; Gao et al., 2011; Huang et al., 2011; Shibazaki et al., 2012). One of the main interests and debates in these studies remains to be the V_P-density (ρ) relationship of Fe alloys at high P–T – does the V_P–ρ relation behave linearly to allow one to extrapolate lower P–T data to Earth's core conditions? In some of the previous studies, the V_P–ρ relations of Fe and its alloys and compounds have been found to behave linearly at ultrahigh pressures and that the high temperature effect was negligible within experimental uncertainties (e.g., Fiquet et al., 2001; Badro et al., 2007; Kantor et al., 2007; Vočadlo 2007; Whitaker et al. 2009; Antonangeli et al., 2012; Murphy et al. 2013; Ohtani et al. 2013). These results have been extensively used to extrapolate experimental results to Earth's core conditions without considering high-temperature effects on the velocity. However, other recent theoretical and experimental results have shown that high temperature causes a significant decrease in the V_P and V_S even at a constant density, indicating that the V_P–ρ relationship of Fe and its alloys needs to be used with caution and experimental results at simultaneous high P–T conditions of the core are needed to reliably decipher the physics and chemistry of the region (Steinle-Neumann et al., 2001; Lin et al., 2005; Sha and Cohen, 2006, 2010; Vočadlo et al., 2009; Gao et al., 2011; Mao et al., 2012). In contrast to these extensive studies on hcp-Fe alloys, experimental results on sound velocities of bcc-Fe and bcc Fe-rich alloys at high P–T remain relatively scarce, calling for further understanding of the elastic behavior of bcc-Fe and Fe-rich light element alloys at high P–T conditions (Klotz and Braden, 2000; Fiquet et al., 2004).

In this study, we have carried out *in situ* HERIX and XRD measurements on polycrystalline bcc-Fe and $Fe_{0.85}Si_{0.15}$ (8 wt.% Si) alloy in an externally-heated diamond anvil cell (EHDAC) at high P–T conditions (Kantor et al., 2012; Mao et al., 2012). The diffraction spectra were used to confirm the crystal structure and the lattice parameters (density) of the bcc phase, while the longitudinal acoustic phonon spectra were used to derive the V_P. These results allow us to reliably establish the V_P–ρ relation of the bcc phase and to understand the alloying effect of Si on the velocity of bcc-Fe. Together with previous studies on the single-crystal elastic constants of the Fe–Si alloy system (Alberts and Wedepohl, 1971; Routbort et al., 1971; Machová and Kadečková, 1977; Petrova et al., 2010), the high P–T and silicon-alloying effects on the V_P and V_S anisotropy of bcc-Fe are analyzed in detail. These results here on the bcc Fe–Si alloys as well as literature values on hcp-Fe alloys are applied to understanding the chemical composition and seismic wave anisotropy of the inner core.

2. Experimental methods

The starting powder Fe and $Fe_{0.85}Si_{0.15}$ alloy were purchased from Alfa Aesar Company with lot H13U044 and Goodfellow Company with lot FE006020/31, respectively. The $Fe_{0.85}Si_{0.15}$ alloy sample has been used and examined in previous XRD and HERIX studies (Lin et al., 2009; Mao et al., 2012). Electron microprobe analyses showed that the Fe sample did not contain any detectable impurities while the Fe–Si alloy contained 7.9 (±0.3) wt.% Si homogeneously. Both samples were polycrystalline in the bcc structure without any observable textures at ambient conditions based on XRD results. The starting sample was pre-selected for its grain size of 1–3 um and slightly pressed between two opposing diamond anvils to form a disk of approximately 60 μm wide and 45 μm thick. A Re gasket of 250 μm thick was pre-indented to 70 μm thick by a pair of diamond anvils with 500 μm culets, and a hole of 250 μm in diameter was then drilled in it. The sample disk was then loaded into the sample chamber of the drilled hole in an EHDAC equipped with a Pt wire heater and a K-type thermocouple (Kantor et al., 2012; Mao et al., 2012). Micro-sized Au powder and a small piece of ruby sphere were placed next to the sample as the primary and secondary pressure calibrant, respectively (Fei et al. 2007; Mao et al., 1986). Ultrahigh purity Ne pressure medium was loaded at 22,000 psi using the high-pressure gas loader in the Mineral Physics Laboratory of the University of Texas at Austin. The temperature of the sample was measured using the K-type thermocouple attached to the pavilion of the diamond close to the sample chamber. The highest temperature of our experiments

was kept at 700 K to allow the bcc phase to remain stable over a wider pressure range (Boehler, 1986; Huang et al., 1987).

High *P–T* HERIX and XRD measurements were conducted using a highly monochromatized incident X-ray beam with an energy of 21.657 keV (0.5725 Å) and an energy bandwidth of 1.2 meV at 3IDC of the Advanced Photon Source (APS), Argonne National Laboratory (ANL) (Toellner et al., 2011). The X-ray beam was focused down to a beamsize of 15 μm vertically and 22 μm horizontally using a set of toroidal and Kirkpatrick–Baez (KB) mirrors in tandem (Alatas et al., 2011). X-ray diffraction patterns of the sample were collected by a digital X-ray flat panel detector (FPDs) from Perkin-Elmer Company before and after experiments, and were integrated using Fit2D Software (Hammersley et al. 1996). The samples remained in the bcc structure in all of our experiments, and no additional diffraction peaks, other than the bcc phase, were observed during and after experiments. The unit cell parameters, densities, and their uncertainties were calculated from two diffraction peaks (1 1 0) and (2 0 0) of the bcc phase, while analyses on the variation of the diffraction intensity as a function of azimuthal angle did not reveal any observable texturing of the bcc samples upon compression (Fig. 1). Pressures and their uncertainties were determined from Au, and were crosschecked via the measured densities of the samples before and after experiments using previously reported equation of state (Mao et al., 1967; Huang et al., 1987; Zhang and Guyot, 1999; Lin et al., 2003a; Fei et al., 2007). For the HERIX experiments, the scattered inelastic signals of the sample were collected and analyzed using a 6-meter long analyzer arm equipped with four spherically-bent silicon crystal analyzers of the (1 8 6 0) reflection working very close to back reflection (89.98°) (Sinn et al., 2001; Alatas et al., 2011). These analyzers were separated by ~3.3 nm^{-1} in the reciprocal space, with an energy resolution of approximately 2.2 meV (Alatas et al., 2011). The collection time for each energy scan was approximately 1 h and about 20 spectra were co-added for each given *P–T* conditions in order to obtain high-quality HERIX spectra of the samples, with very small temperature fluctuation less than 1 K.

3. Results and data analyses

HERIX spectra of the bcc-Fe were collected at four different momentum transfers (*Q*) of 4.0, 7.3, 10.6 and 13.9 nm^{-1} up to 11 GPa at three given temperatures (300 K, 500 K, and 700 K) (Fig. 2 and Table 1), while the spectra for bcc-$Fe_{0.85}Si_{0.15}$ were collected at high pressures and room temperature. Measured longitudinal acoustic (*LA*) phonon dispersion curves of the samples were

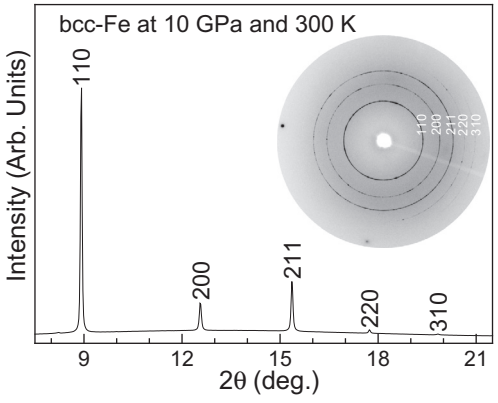

Fig. 1. Representative X-ray diffraction pattern of bcc-Fe at 10 GPa and 300 K. Insert, original diffraction image. An incident X-ray wavelength of λ = 0.3100 Å was used for the measurement at the GeoSoilEnviroCARS of the APS. The sample was in the bcc phase and did not exhibit any observable textures.

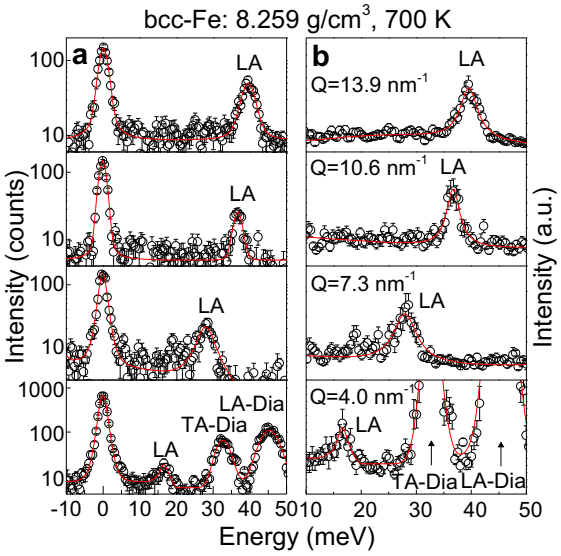

Fig. 2. Representative HERIX spectra of bcc-Fe as a function of momentum transfer (*Q*) at 11 GPa and 700 K. (a) The full-profile HERIX spectra in the logarithmic scale. (b) The HERIX spectra of the interesting region shown in the linear scale. Experimental data (open circles with error bars) were fitted with a Lorentzian function (solid lines) for the longitudinal acoustic phonon peak (*LA*). Transverse acoustic (*TA-Dia*) and longitudinal acoustic phonon peaks (*LA-Dia*) from diamond anvils were observed when the momentum transfer (*Q*) was at 4.0 nm^{-1}.

Table 1
Compressional wave velocity and density of polycrystalline bcc-Fe and $Fe_{0.85}Si_{0.15}$ at high pressures and temperatures.

V_P (km/s)	ρ (g/cm^3)	P (GPa)*
bcc-Fe (300 K)		
5.97 (±0.05)	7.877 (±0.002)	1 bar
6.11 (±0.05)	7.965 (±0.003)	1.9 (±0.2)
6.28 (±0.03)	8.065 (±0.003)	4.2 (±0.3)
6.45 (±0.06)	8.187 (±0.002)	7.4 (±0.5)
6.58 (±0.05)	8.311 (±0.005)	10.3 (±0.5)
bcc-Fe (500 K)		
6.02 (±0.05)	7.945 (±0.002)	3.1 (±0.3)
6.22 (±0.06)	8.092 (±0.003)	6.6 (±0.5)
6.40 (±0.05)	8.217 (±0.003)	9.7 (±0.5)
bcc-Fe (700 K)		
5.67 (±0.04)	7.742 (±0.004)	1 bar
5.94 (±0.07)	7.937 (±0.002)	3.8 (±0.3)
6.18 (±0.06)	8.121 (±0.003)	8.0 (±0.5)
6.38 (±0.08)	8.259 (±0.004)	10.9 (±0.5)
$Fe_{0.85}Si_{0.15}$ (300 K)		
6.19 (±0.05)	7.398 (±0.002)	1 bar
6.40 (±0.06)	7.515 (±0.005)	2.5 (±0.2)
6.85 (±0.07)	7.819 (±0.006)	9.0 (±0.4)
7.13 (±0.09)	7.996 (±0.006)	14.5 (±0.5)

* Neon was used as the pressure-transmitting medium. Pressures were calculated from Au (Fei et al., 2007), and were crosschecked using the equation of state (EoS) of bcc-Fe (Mao et al., 1967; Huang et al., 1987) and bcc-$Fe_{0.85}Si_{0.15}$ (Lin et al., 2003a).

fitted to a sine function of the momentum (*Q*) and energy transfers (*E*) to derive the compressional-wave velocity (V_P) (Fig. 3) (see Fiquet et al. (2004) and Kantor et al. (2007) for further details). The uncertainty of the derived V_P is approximately 1% (Table 1), allowing us to better constrain high *P–T* and silicon-alloying effects on the V_P of the bcc-Fe. We note that the elastic peaks in the HERIX spectra are typically much stronger than the longitudinal acoustic phonon peaks of bcc-Fe and bcc-$Fe_{0.85}Si_{0.15}$ at the lowest Q (4 nm^{-1}).

Given the limited density (pressure) range (approximately 0.4 g/cm^3 increase in density) of our experiments, the derived V_P–ρ profiles of the bcc-Fe and $Fe_{0.85}Si_{0.15}$ at each given temperature can be well represented by a linear function. The V_P of

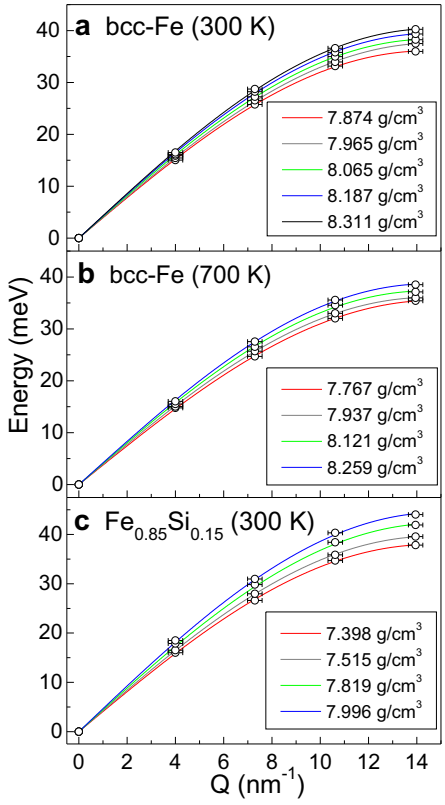

Fig. 3. Longitudinal acoustic phonon dispersion curves of bcc-Fe (a, b) and bcc-$Fe_{0.85}Si_{0.15}$ (c) at high pressures. The measured momentum–energy (Q–E) relations (open circles) were fitted using a sine function (solid lines). The energy and momentum transfers at the origin of the first Brillouin zone are intrinsically set at zero for the data analyses. Errors (±1σ) for the momentum transfer are typically in the order of 0.3 nm^{-1}, while uncertainties for the energy transfer are mostly less than 1%. Errors smaller than the symbols are not shown for clarity.

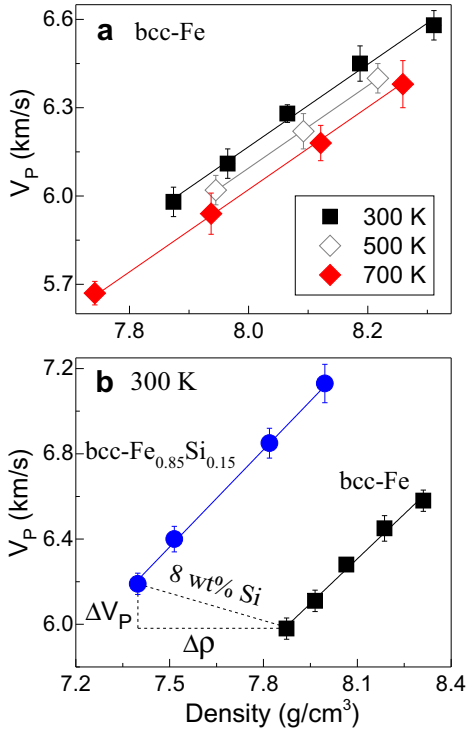

Fig. 4. Compressional wave velocity (V_P) and density (ρ) relations of bcc-Fe (a) and bcc Fe–Si alloy (b) at high pressures and temperatures. Solid lines: linear fits of the experimental data. Dashed lines illustrate the alloying effect of 8 wt.% Si on the V_P–ρ relation of bcc-Fe at ambient conditions in which the velocity increase at a constant density (ΔV_P) and the density decrease ($\Delta\rho$) at a constant velocity are shown respectively.

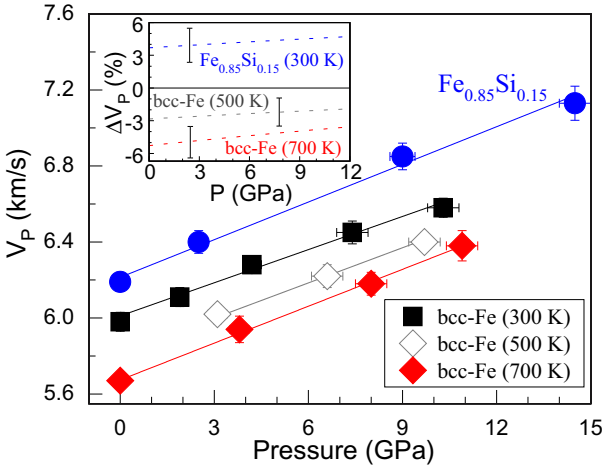

Fig. 5. Compressional wave velocity (V_P) of bcc-Fe and bcc-$Fe_{0.85}Si_{0.15}$ as a function of pressure. Solid lines: linear fits of the experimental data; solid circles: bcc-$Fe_{0.85}Si_{0.15}$ at 300 K. Insert: velocity deviation (ΔV_P (%)) as a function of pressure using the experimental V_P of bcc-Fe at 300 K ($V_{P,300}$) as the reference. The deviation is defined as: $\Delta V_P\,(\%) = ((V_P - V_{P,300}) / V_{P,300}) \times 100$. Dashed lines: linear fits of the derived velocity deviation; vertical ticks: representative errors (±1σ) are calculated using standard error propagations.

bcc-Fe measured at elevated temperatures was clearly reduced, even at a constant density (Fig. 4a). For example, at a constant density of 7.877 (±0.002) g/cm^3, the V_P of the bcc-Fe was reduced by 2.2 (±1.6)% from 300 K to 700 K. The velocity reduction at our maximum density of 8.311 (±0.005) g/cm^3 was 1.2 (±0.9)% from 300 K to 700 K, which appears to be smaller than that at lower densities; however, our data uncertainty within a limited temperature range does not permit us to further infer the higher-density effect on the temperature-reduced velocity decrease reported previously for hcp-Fe and Fe–Si alloy (Mao et al., 2012). On the other hand, at ambient pressure, the velocities of bcc-Fe at 500 K and 700 K were lower than that at 300 K by 2.9 (±1.6)% and 5.1 (±1.9)%, respectively (Fig. 5 insert). We note that the V_P reduction at high temperatures and at a given density has been reported in recent NRIXS and HERIX studies for hcp-Fe (Lin et al., 2005; Mao et al., 2012). Compared with V_P–ρ profile of the bcc-Fe at 300 K, the $Fe_{0.85}Si_{0.15}$ alloy systematically exhibits much higher V_P and lower ρ (Figs. 4b and 5). The addition of 8 wt.% Si into bcc-Fe results in a density reduction ($\Delta\rho$) by approximately 7.6% and a velocity increase (ΔV_P) by 3.6 (±1.6)% at ambient P–T conditions, while the $\Delta\rho$ was approximately 7.2% and the ΔV_P was 5.0 (2.1)% at the maximum pressure of 15 GPa.

4. Discussions and implications

4.1. High P–T effects on V_P of the bcc-Fe

Our V_P–ρ profiles of the bcc-Fe and Fe–Si alloy are used to decipher the high P–T and silicon-alloying effects on the velocity profile of iron. As stated earlier, the linear V_P–ρ relationship, so called Birch's law, has been widely used to extrapolate experimental data at limited P–T range to Earth's core conditions (e.g., Fiquet et al., 2001; Badro et al., 2007; Kantor et al., 2007; Antonangeli et al., 2010, 2012). This linear approximation was empirically observed by Francis Birch (1961a,b) to correlate the bulk sound velocity and density results in shockwave experiments, in which the wave

velocity and density behave approximately linearly along a Hugoniot for materials with common mean atomic weights (e.g., Birch, 1961a,b; McQueen et al., 1964; Wang, 1970; Vočadlo, 2007). However, a number of previous studies have shown that the linear approximation is only a manifestation of the power-law relation over a limited density range (Anderson, 1967, 1973; Chung, 1972; Shankland, 1972; Liebermann and Ringwood, 1973; Mao et al., 2012), and that the linear behavior does not hold through a structural phase transition (Campbell and Heinz, 1992). Furthermore, temperature-dependent velocity of the hcp-Fe and its alloys as a function of density has been recently reported experimentally and theoretically (e.g., Steinle-Neumann et al., 2001; Lin et al., 2005; Sha and Cohen, 2006, 2010; Kantor et al., 2007; Vočadlo, 2007; Vocadlo et al., 2009; Gao et al., 2011; Mao et al., 2012; Antonangeli et al., 2012; Murphy et al. 2013; Ohtani et al. 2013).

The V_P–ρ and V_P–P profiles of our bcc-Fe at given temperatures display an evident V_P reduction with increasing temperature even at a constant density (Figs. 4 and 5), showing a strong temperature effect on the V_P. Compared with the V_P reduction of 5.4% for the hcp-Fe of 9.256 g/cm^3 at 700 K (Mao et al., 2012), the overall V_P reduction of bcc-Fe was much smaller at 700 K, suggesting that the elasticity of bcc and hcp phases can behave quite differently at high P–T conditions (see further discussions in next paragraph). Lin et al. (2005) have reported sound velocities of hcp-Fe up to 1700 K at moderate pressures which showed the strong temperature-dependent V_P and V_S. The V_S of Fe_3C also showed a strong temperature-dependence up to approximately 1450 K and 47 GPa (Gao et al., 2011). Moreover, first-principles calculations found that at a fixed density, the shear-wave velocity (V_S) of hcp-Fe decreases approximately by half from 0 K to 6000 K (Steinle-Neumann et al., 2001). In contrast, Antonangeli et al. (2012) suggested no such temperature reduction in the hcp-Fe up to 1100 K and 93 GPa, although their V_P measurements at approximately 900 K and 9.5 g/cm^3 appear to be below their linear fitting line.

To further demonstrate the high-temperature effect on the V_P, we have analyzed the V_P–ρ relationship of bcc-Fe from 0 K to 1185 K using literature and our results (Dever, 1972; Isaak and Masuda, 1995; Adams et al., 2006). We note that the literature V_P presented here represents the polycrystalline V_P of the sample as derived from single-crystal elastic constants using the Voigt–Reuss–Hill average method by Hill (1952). The ferromagnetic (FM) bcc-Fe is stable up to the Curie temperature (T_C) of 1043 K, and its V_P–ρ profile follows a non-linear function and can be well represented using the power-law function (Fig. 6):

$$V_P = C(M)(\rho + \alpha(T))^{\lambda} \quad (1)$$

where $C(M)$ is an atomic mass constant at a given temperature, $a(T)$ is a temperature-dependent correction factor, and λ is a correction factor for the non-linear behavior of the V_P–ρ relationship (see Mao et al. (2012) for further details). In our power-law fitting for the V_P–ρ relation, the FM phase exhibits $C(M) = 6.484$ (±0.031), $a(T) = -7.552$ (±0.014), and $\lambda = 0.0804$ (±0.0063). Above 1043 K, the bcc-Fe undergoes a ferromagnetic to paramagnetic (PM) transition that is also associated with a discontinuity in the V_P–ρ profile. The V_P–ρ relation of the PM phase can be simply fitted with the linear function ($V_P = 3.833$ (±0.046) ρ – 24.01 (±0.35)), instead of the power-law function behavior for the FM phase. These analyses here strongly support the notion that high temperature and magnetism have a strong effect on the V_P of Fe and that the V_P–ρ profile of Fe can be affected by structural and magnetic transitions (Fig. 6). Our bcc-Fe and Fe–Si alloy at high P–T is likely in the FM state and their V_P–ρ profiles may thus be affected by various degrees of magnetism resulting in different V_P–ρ profiles than the non-magnetic counterparts at high P–T conditions relevant to the Earth's core (e.g., Steinle-Neumann et al., 2004; Belonoshko et al., 2008b; Ruban et al., 2013). Analyses of the V_P of bcc-Fe as a function of the frequency of the experimental probes including ultrasonic and HERIX techniques show that the V_P slightly increases with frequency of the probe, suggesting a potential frequency-dependent velocity in the system, although these ambient data are consistent within uncertainty (Fig. 6 insert) (e.g., Isaak and Masuda, 1995).

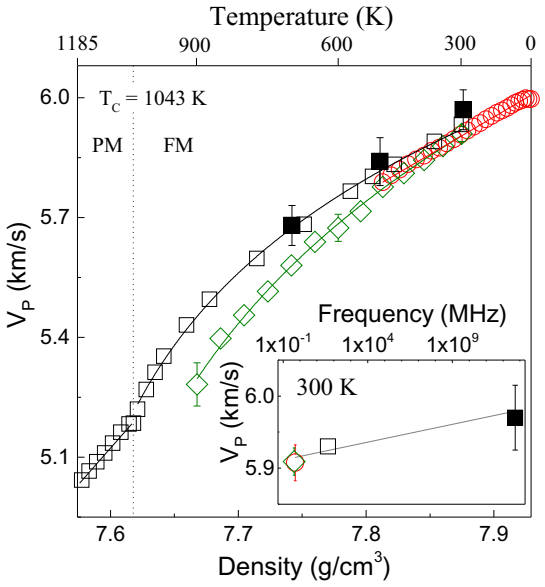

Fig. 6. Compressional wave velocity (V_P) of bcc-Fe as a function of density (temperature) at ambient pressure (0.1 MPa). Solid squares: this study; open circles: polycrystalline V_P calculated from the elastic constants (using the Voigt–Reuss–Hill average method by Hill (1952)) measured by the ultrasonic techniques at the frequencies of 0.3–0.75 MHz (Adams et al., 2006); open diamonds: ultrasonic data at 0.3–0.6 MHz (Isaak and Masuda, 1995); open squares: ultrasonic data at 20–70 MHz (Dever, 1972). A power-law function (Mao et al., 2012) is used to fit the V_P–ρ relation of the ferromagnetic (FM) bcc-Fe between 300 K and the critical temperature (T_C) of 1043 K, whereas the V_P–ρ relation for the paramagnetic (PM) bcc-Fe can be well represented by a linear function. The insert figure shows the frequency dependence of the V_P at 300 K. Vertical ticks represent experimental errors (±1σ).

4.2. Alloying effect of Si on the velocity–density profile of bcc-Fe

To understand the alloying effects of Si on the sound velocity of the bcc-Fe, we have also compared our results to literature values on bcc-Fe and Fe–Si alloys at high pressures (Guinan and Beshers, 1968; Alberts and Wedepohl, 1971; Routbort et al., 1971; Dever, 1972; Machová and Kadečková, 1977; Isaak and Masuda, 1995; Adams et al., 2006; Badro et al., 2007; Zhang et al., 2010; Petrova et al., 2010). These results show that Fe–Si alloys systematically exhibit higher polycrystalline V_P and lower ρ than pure Fe for both bcc and hcp phases (Figs. 4b and 8a) (Fiquet et al., 2001, 2004; Lin et al., 2003b; Antonangeli et al., 2004, 2010, 2012; Badro et al., 2007; Tsuchiya and Fujibuchi, 2009; Mao et al., 2012). The V_P–ρ profile of bcc-$Fe_{0.85}Si_{0.15}$ exhibits similar high-pressure behavior to bcc-Fe via a constant density offset. That is, the V_P–ρ profile of the bcc-$Fe_{0.85}Si_{0.15}$ would match well with that of the bcc-Fe by a density decrease of 0.6 g/cm^3 as a result of lighter Si addition (Fig. 4b). We note that the V_P-ρ profile of FeSi (33.5 wt.% Si) also shows similar high-pressure behavior to bcc-Fe via a constant density offset of ~2.3 g/cm^3 (Badro et al., 2007) (Fig. 7b).

Based on our experimental HERIX and previous ultrasonic results, the V_P of bcc-Fe slightly increases with increasing Si content in the Fe-rich Fe–Si alloys system at ambient conditions (Fig. 7a) (Guinan and Beshers, 1968; Alberts and Wedepohl, 1971; Routbort et al., 1971; Dever, 1972; Machová and

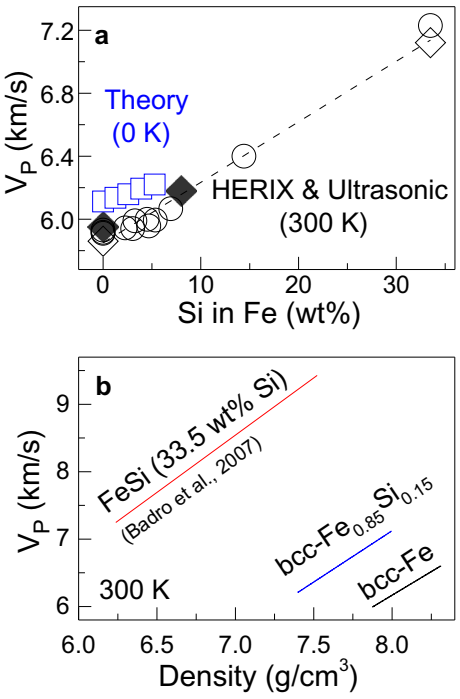

Fig. 7. Compressional wave velocity of the Fe–Si alloy. (a) V_P as a function of Si content (wt.%) at ambient pressure; (b) V_P as a function of density at high pressures and 300 K. Solid diamonds: HERIX at ambient conditions (this study); open diamonds: HERIX at ambient conditions (Fiquet et al., 2004); open squares: theoretical calculation at 0 K (Zhang et al. 2010); open circles: ultrasonic measurements at ambient conditions (Guinan and Beshers, 1968; Alberts and Wedepohl, 1971; Routbort et al., 1971; Dever, 1972; Machová and Kadečková, 1977; Isaak and Masuda, 1995; Adams et al., 2006; Petrova et al., 2010). Dashed lines are linear fits to the data. Errors are smaller than the symbols and are not shown for clarity.

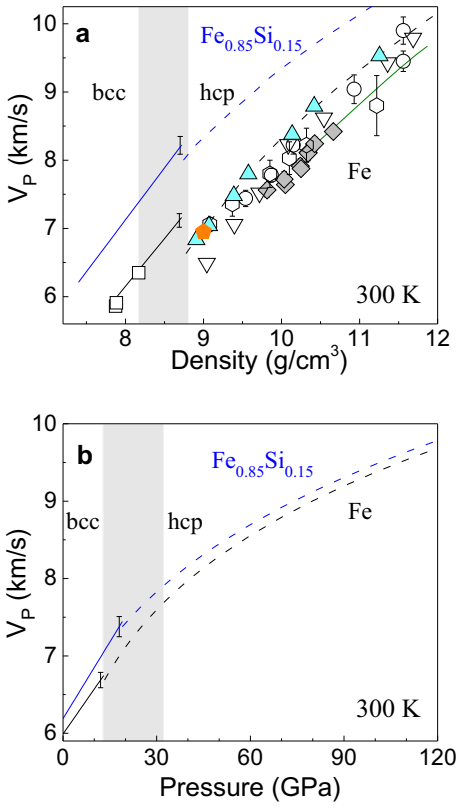

Fig. 8. V_P–ρ (a) and V_P–P profiles (b) of Fe and $Fe_{0.85}Si_{0.15}$ in the bcc and hcp structure at 300 K. Blue and black solid lines: bcc-$Fe_{0.85}Si_{0.15}$ and bcc-Fe, respectively (this study); blue and black dashed lines: hcp-$Fe_{0.85}Si_{0.15}$ and hcp-Fe, HERIX (Mao et al., 2012); olivine solid line: hcp-Fe, shockwave experiments (Brown and McQueen, 1986); open squares: bcc-Fe, HERIX (Fiquet et al., 2001, 2004); solid pentagons: hcp-Fe, ultrasonic (Mao et al., 1998); open hexagons: hcp-Fe, HERIX (Fiquet et al., 2001); open circles: hcp-Fe, HERIX (Antonangeli et al., 2004, 2012); open triangles: hcp-Fe, NRIXS (Mao et al., 2001); solid triangles: hcp-Fe, ISLS (Crowhurst et al., 2004); solid diamonds: hcp-Fe, NRIXS (Lin et al., 2005). (For interpretation of the references to color in this figure legend, the reader is referred to the web version of this article.)

Kadečková, 1977; Isaak and Masuda, 1995; Adams et al., 2006). Theoretical calculations on Fe-rich Fe–Si alloys at 0 K also show a similar behavior (Zhang et al., 2010). These findings on this velocity–density behavior of Fe–Si alloys clearly validates the notion that addition of Si in bcc-Fe mainly contributes to the density deficit at high pressures while the velocity is less affected by the alloying light element (Lin et al., 2003a,b; Mao et al., 2012). We note that the Si-rich counterpart also exhibits a linear relationship between the V_P–Si content up to 33.5 wt.% at ambient conditions, suggesting that our results on bcc Fe and $Fe_{0.85}Si_{0.15}$ (8 wt.% Si) should be appropriately applied to higher Si content if the Earth's core or the interiors of other planetary bodies contain Si-rich Fe–Si alloys.

4.3. V_P–ρ profile across the bcc–hcp phase transition

Comparison of the V_P–ρ results between the bcc and hcp phases of Fe and Fe-rich Fe–Si alloys illustrates a V_P–ρ discontinuity through the bcc–hcp structural transition (Fig. 8a) (Mao et al., 2001; Fiquet et al., 2001; Lin et al., 2003b; Mao et al., 2012), showing that Birch's law does not hold through a phase transition (Campbell et al., 1992). We should note that the discontinuity in the V_P–ρ plot can be attributed the density jump of approximately 5% through the bcc–hcp phase transition (Mao et al., 1967; Lin et al., 2003a) (Fig. 8b). We note that the hcp-Fe loses its magnetism across the bcc–hcp transition which may also contribute to some changes in the V_P–ρ profile (Steinle-Neumann et al., 2004) (Figs. 6 and 8a). The bcc phase exhibits a higher V_P–ρ profile than the hcp phase, although the V_P–ρ profiles of Fe and Fe–Si alloys appear to be similar. This behavior, along with the linear compositional effect of Si on the V_P of Fe shown in Fig. 7, indicates that the compositional effect of Si may be linearly scaled with the Si content (Zhang and Guyot, 1999). Assuming this trend remains valid in the inner core conditions, the presence of the bcc-structured Fe–Si alloy in the inner core would manifest seismically with a higher V_P–ρ profile than that of the hcp phase, requiring lesser amounts of light elements to match the density deficits of the inner core (Belonoshko et al., 2003, 2008a,b).

4.4. Compressional and shear wave anisotropy of bcc Fe–Si alloys

Single-crystal elastic constants of Fe–Si alloys have been previously reported as a function of temperature and Si content using ultrasonic interferometer measurements (Lord and Beshers, 1965; Guinan and Beshers, 1968; Dever, 1972; Isaak and Masuda, 1995; Adams et al., 2006). These results are re-analyzed to help understand elastic anisotropies of bcc Fe–Si alloys at high P–T conditions. The anisotropy factor (A) is calculated using the single-crystal elastic constants of bcc-Fe and Fe–Si alloys following the method in Mainprice et al. (2000):

$$A = 2 \times ((V_{max} - V_{min})/(V_{max} + V_{min})) \times 100\% \quad (2)$$

where V_{max} and V_{min} represent the maximum and minimum V_P and V_S velocities of bcc-Fe and Fe–Si alloys, respectively. bcc-Fe exhibits V_P anisotropy of 16 (±2)% and V_S splitting anisotropy of 42 (±3)% at ambient conditions (Fig. 9a). The V_P and V_S anisotropies increase to

25 (±2)% and 75 (±3)%, respectively, with increasing temperature up to 1043 K (T_C). The magnetic transition from the FM to PM states of bcc-Fe at approximately 1043 K also enhances the V_S anisotropy while the V_P anisotropy is less affected by such a transition (Fig. 9a). That is, the magnetic transition would not affect velocity anisotropies of bcc-Fe. On the other hand, theoretical (Sha and Cohen, 2006) and experimental (Klotz and Braden, 2000) results showed that the anisotropy of bcc-Fe almost remains constant with increasing pressure up to 10 GPa at room temperature (Fig. 9b). The addition of Si into bcc-Fe with Si content up to 7 wt.% also enhances the V_P and V_S anisotropy of bcc-Fe to 22 (±2)% and 61 (±3)% at ambient conditions, respectively (Fig. 9c). Considering the combined effects of high P–T and the addition of Si in bcc-Fe, it is conceivable that bcc Fe–Si alloy likely exhibits extremely strong V_P and V_S anisotropies at high P–T. If such strong V_P and V_S anisotropies persist to the extreme conditions of the Earth's core, a certain amount of bcc-Fe alloyed with light elements with preferred orientations may produce elastic anisotropies that could be used to explain the observed seismic anisotropy in the region (Belonoshko et al., 2008a).

In summary, our results here confirmed the observations that high temperature has evident effects on sound velocities of Fe (Lin et al., 2005; Gao et al., 2011; Mao et al., 2012). We also found that by adding Si into bcc-Fe, the bcc Fe–Si alloys display similar high-pressure behavior via a constant density offset, indicating that a small amount of Si light element is likely incorporated into the inner core. Based on literature results of the compressional and shear wave anisotropy of bcc-Fe as a function of P–T and Si content, bcc-structured Fe–Si alloy crystals with preferred orientations may potentially produce the observed seismic anisotropy of the inner core.

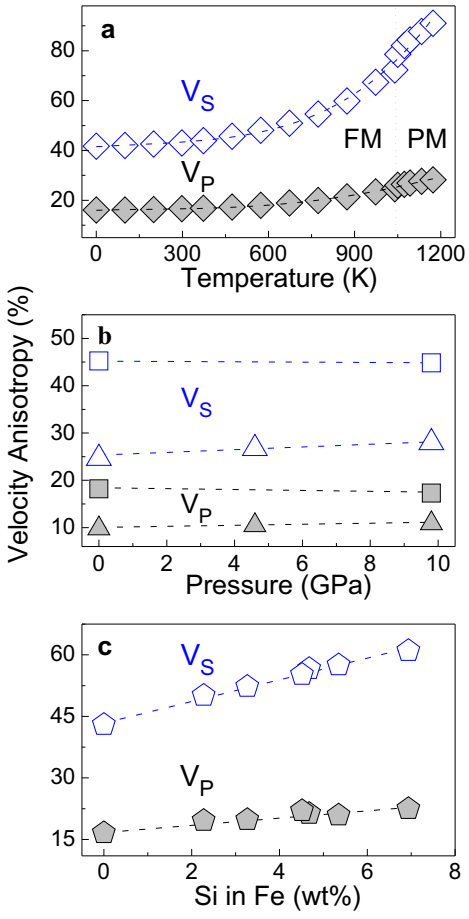

Fig. 9. Compressional-wave (V_P) and shear-wave (V_S) anisotropy of bcc-Fe as a function of temperature, pressure, and Si content. The anisotropy factor (A) is given in the Eq. (2) in the text. (a) Ultrasonic measurements on bcc-Fe at ambient pressure (Lord and Beshers, 1965; Guinan and Beshers, 1968; Dever, 1972; Isaak and Masuda, 1995; Adams et al., 2006); (b) squares: inelastic neutron scattering (INS) measurements at 300 K (Klotz and Braden, 2000); triangles: theoretical calculations at 250 K (Sha and Cohen, 2006); (c) ultrasonic measurements on Fe-rich Fe–Si alloys at ambient conditions (Alberts and Wedepohl, 1971; Dever, 1972; Machová and Kadecková, 1977). Dashed lines: fits to the data. Errors smaller than the symbols are not shown for clarity.

Acknowledgments

We thank J. Zhu, J. Zhao, and D. Fan for experimental assistance. We are grateful to X. Wu, J. Yang, and B. Chen for their helpful discussions and L. Dafov for editing the manuscript. J. F. Lin acknowledges supports from the U.S. National Science Foundation (EAR-1053446 and EAR-1056670) and the Carnegie/DOE Alliance Center (CDAC). We also thank HPCAT and GeoSoilEnviroCARS of the APS, ANL for the use of the optical ruby and diffraction systems and the Keithley thermometer. GeoSoilEnviroCARS (Sector 13) is supported by the National Science Foundation – Earth Sciences (EAR-1128799), and the Department of Energy, Geosciences (DE-FG02-94ER14466). Use of the Advanced Photon Source, an Office of Science User Facility operated for the U.S. Department of Energy (DOE) Office of Science by Argonne National Laboratory, is supported by the U.S. DOE under Contract No. DE-AC02-06CH11357.

References

Adams, J.J., Agosta, D.S., Leisure, R.G., Ledbetter, H., 2006. Elastic constants of monocrystal iron from 3 to 500 K. J. Appl. Phys. 100, 113530–113537.
Alatas, A., Leu, B.M., Zhao, J., Yavaş, H., Toellner, T.S., Alp, E.E., 2011. Improved focusing capability for inelastic X-ray spectrometer at 3-ID of the APS: a combination of toroidal and Kirkpatrick-Baez (KB) mirrors. Nucl. Instrum. Meth. A 649, 166–168.
Alberts, H.L., Wedepohl, P.T., 1971. Elastic constants of dilute iron–silicon alloy single crystals below room temperature. Physica 53, 571–580.
Alfè, D., Gillan, M.J., Price, G.D., 2002. Composition and temperature of the Earth's core constrained by combining ab initio calculations and seismic data. Earth Planet. Sci. Lett. 195, 91–98.
Anderson, D.L., 1967. A seismic equation of state. Geophys. J. Int. 13, 9–30.
Anderson, O.L., 1973. Comments on the power law representation of Birch's law. J. Geophys. Res. 78, 4901–4914.
Antonangeli, D., Occelli, F., Requardt, H., Badro, J., Fiquet, G., Krisch, M., 2004. Elastic anisotropy in textured hcp-iron to 112 GPa from sound wave propagation measurements. Earth Planet. Sci. Lett. 225, 243–251.
Antonangeli, D., Siebert, J., Badro, J., Farber, D.L., Fiquet, G., Morard, G., Ryerson, F.J., 2010. Composition of the Earth's inner core from high-pressure sound velocity measurements in Fe–Ni–Si alloys. Earth Planet. Sci. Lett. 295, 292–296.
Antonangeli, D., Komabayashi, T., Occelli, F., Borissenko, E., Walters, A.C., Fiquet, G., Fei, Y., 2012. Simultaneous sound velocity and density measurements of hcp iron up to 93 GPa and 1100 K: an experimental test of the Birch's law at high temperature. Earth Planet. Sci. Lett. 331–332, 210–214.
Asanuma, H., Ohtani, E., Sakai, T., Terasaki, H., Kamada, S., Kondo, T., Kikegawa, T., 2010. Melting of iron–silicon alloy up to the core–mantle boundary pressure: implications to the thermal structure of the Earth's core. Phys. Chem. Miner. 37, 353–359.
Badro, J., Fiquet, G., Guyot, F., Gregoryanz, E., Occelli, F., Antonangeli, D., d'Astuto, M., 2007. Effect of light elements on the sound velocities in solid iron: implications for the composition of Earth's core. Earth Planet. Sci. Lett. 254, 233–238.
Belonoshko, A.B., Ahuja, R., Johansson, B., 2003. Stability of the body-centred-cubic phase of iron in the Earth's inner core. Nature 424, 1032–1034.
Belonoshko, A.B., Isaev, E.I., Skorodumova, N.V., Johansson, B., 2006. Stability of the body-centered-tetragonal phase of Fe at high pressure: ground-state energies, phonon spectra, and molecular dynamics simulations. Phys. Rev. B 74, 214102.
Belonoshko, A.B., Skorodumova, N.V., Rosengren, A., Johansson, B., 2008a. Elastic anisotropy of Earth's inner core. Science 319, 797–800.
Belonoshko, A.B., Dorogokupets, P.I., Johansson, B., Saxena, S.K., Koči, L., 2008b. Ab initio equation of state for the body-centered-cubic phase of iron at high pressure and temperature. Phys. Rev. B 78, 104107.
Belonoshko, A.B., Derlet, P.M., Mikhaylushkin, A.S., Simak, S.I., Hellman, O., Burakovsky, L., Swift, D.C., Johansson, B., 2009. Quenching of bcc-Fe from high to room temperature at high-pressure conditions: a molecular dynamics simulation. New J. Phys. 11, 093039.

Belonoshko, A.B., Arapan, S., Rosengren, A., 2011. An ab initio molecular dynamics study of iron phases at high pressure and temperature. J. Phys.: Condens. Matter 23, 485402.

Birch, F., 1952. Elasticity and constitution of the Earth's interior. J. Geophys. Res. 57, 227–286.

Birch, F., 1961a. Composition of the Earth's mantle. Geophys. J. R. Astron. Soc. 4, 295–311.

Birch, F., 1961b. The velocity of compressional waves in rocks to 10 Kilobars, part 2. J. Geophys. Res. 66, 2199–2224.

Birch, F., 1964. Density and composition of mantle and core. J. Geophys. Res. 69, 4377–4388.

Boehler, R., 1986. The phase diagram of iron to 430 kbar. Geophys. Res. Lett. 13, 1153–1156.

Brown, J.M., McQueen, R.G., 1986. Phase transitions, Grüneisen parameter, and elasticity for shocked iron between 77 GPa and 400 GPa. J. Geophys. Res. 91, 7485–7494.

Campbell, A.J., Heinz, D.L., 1992. A high-pressure test of Birch's law. Science 257, 66–68.

Chen, B., Li, J., Hauck, S.A., 2008. Non-ideal liquidus curve in the Fe–S system and Mercury's snowing core. Geophys. Res. Lett. 35, L07201.

Chung, D.H., 1972. Birch's law: why is it so good? Science 177, 261–263.

Côté, A.S., Vočadlo, L., Brodholt, J.P., 2008. The effect of silicon impurities on the phase diagram of iron and possible implications for the Earth's core structure. J. Phys. Chem. Solids 69, 2177–2181.

Côté, A.S., Vočadlo, L., Dobson, D.P., Alfè, D., Brodholt, J.P., 2010. Ab initio lattice dynamics calculations on the combined effect of temperature and silicon on the stability of different iron phases in the Earth's inner core. Phys. Earth Planet. Inter. 178, 2–7.

Crowhurst, J.C., Goncharov, A.F., Zaug, J.M., 2004. Impulsive stimulated light scattering from opaque materials at high pressure. J. Phys.: Condens. Matter 16, S1137.

Cui, H., Zhang, Z., Zhang, Y., 2013. The effect of Si and S on the stability of bcc iron with respect to tetragonal strain at the Earth's inner core conditions. Geophys. Res. Lett. 40, 2958–2962.

Dever, D.J., 1972. Temperature dependence of the elastic constants in alpha-iron single crystals: relationship to spin order and diffusion anomalies. J. Appl. Phys. 43, 3293–3301.

Dubrovinsky, L., Dubrovinskaia, N., Narygina, O., Kantor, I., Kuznetzov, A., Prakapenka, V.B., Vitos, L., Johansson, B., Mikhaylushkin, A.S., Simak, S.I., Abrikosov, I.A., 2007. Body-centered cubic iron-nickel alloy in Earth's core. Science 316, 1880–1883.

Dubrovinsky, L., Lin, J.-F., 2009. Mineral physics quest to the Earth's core. Eos. Trans. Am. Geophys. Union 90, 21–22.

Fei, Y., Ricolleau, A., Frank, M., Mibe, K., Shen, G., Prakapenka, V., 2007. Toward an internally consistent pressure scale. Proc. Natl. Acad. Sci. U.S.A 104, 9182–9186.

Fiquet, G., Badro, J., Guyot, F., Requardt, H., Krisch, M., 2001. Sound velocities in iron to 110 gigapascals. Science 291, 468–471.

Fiquet, G., Badro, J., Guyot, F., Bellin, C., Krisch, M., Antonangeli, D., Requardt, H., Mermet, A., Farber, D., Aracne-Ruddle, C., Zhang, J., 2004. Application of inelastic X-ray scattering to the measurements of acoustic wave velocities in geophysical materials at very high pressure. Phys. Earth Planet. Inter. 143–144, 5–18.

Fischer, R.A., Campbell, A.J., Reaman, D.M., Miller, N.A., Heinz, D.L., Dera, P., Prakapenka, V.B., 2013. Phase relations in the Fe–FeSi system at high pressures and temperatures. Earth Planet. Sci. Lett. 373, 54–64.

Gao, L., Chen, B., Zhao, J., Alp, E.E., Sturhahn, W., Li, J., 2011. Effect of temperature on sound velocities of compressed Fe_3C, a candidate component of the Earth's inner core. Earth Planet. Sci. Lett. 309, 213–220.

Geballe, Z.M., Lasbleis, M., Cormier, V.F., Day, E.A., 2013. Sharp hemisphere boundaries in a translating inner core. Geophys. Res. Lett. 40, 1719–1723.

Guinan, M.W., Beshers, D.N., 1968. Pressure derivatives of the elastic constants of α-iron to 10 kbs. J. Phys. Chem. Solids 29, 541–549.

Hammersley, A.P., Svensson, S.O., Hanfland, M., Fitch, A.N., Hausermann, D., 1996. Two-dimensional detector software: From real detector to idealised image or two-theta scan. High Press. Res. 14, 235–248.

Hill, R., 1952. The elastic behaviour of a crystalline aggregate. Proc. Phys. Soc. A 65, 349.

Hirao, N., Ohtani, E., Kondo, T., Kikegawa, T., 2004. Equation of state of iron–silicon alloys to megabar pressure. Phys. Chem. Miner. 31, 329–336.

Huang, E., Bassett, W.A., Tao, P., 1987. Pressure-temperature-volume relationship for hexagonal close packed iron determined by synchrotron radiation. J. Geophys. Res. 92, 8129–8135.

Huang, H., Fei, Y., Cai, L., Jing, F., Hu, X., Xie, H., Zhang, L., Gong, Z., 2011. Evidence for an oxygen-depleted liquid outer core of the Earth. Nature 479, 513–516.

Isaak, D.G., Masuda, K., 1995. Elastic and viscoelastic properties of α iron at high temperatures. J. Geophys. Res. 100, 17689–17698.

Kantor, A.P., Kantor, I.Y., Kurnosov, A.V., Kuznetsov, A.Y., Dubrovinskaia, N.A., Krisch, M., Bossak, A.A., Dmitriev, V.P., Urusov, V.S., Dubrovinsky, L.S., 2007. Sound wave velocities of fcc Fe–Ni alloy at high pressure and temperature by mean of inelastic X-ray scattering. Phys. Earth Planet. Inter. 164, 83–89.

Kantor, I., Prakapenka, V., Kantor, A., Dera, P., Kurnosov, A., Sinogeikin, S., Dubrovinskaia, N., Dubrovinsky, L., 2012. BX90: a new diamond anvil cell design for X-ray diffraction and optical measurements. Rev. Sci. Instrum. 83, 125102–125106.

Klotz, S., Braden, M., 2000. Phonon dispersion of bcc iron to 10 GPa. Phys. Res. Lett. 85, 3209–3212.

Kuwayama, Y., Hirose, K., Sata, N., Ohishi, Y., 2008. Phase relations of iron and iron–nickel alloys up to 300 GPa: implications for composition and structure of the Earth's inner core. Earth Planet. Sci. Lett. 273, 379–385.

Kuwayama, Y., Sawai, T., Hirose, K., Sata, N., Ohishi, Y., 2009. Phase relations of iron–silicon alloys at high pressure and high temperature. Phys. Chem. Miner. 36, 511–518.

Li, J., Fei, Y., 2003. Experimental constraints on core composition. Treatise Geochem. 2, 521–546.

Liebermann, R.C., Ringwood, A.E., 1973. Birch's law and polymorphic phase transformations. J. Geophys. Res. 78, 6926–6932.

Lin, J.-F., Heinz, D.L., Campbell, A.J., Devine, J.M., Shen, G., 2002. Iron–silicon alloy in Earth's core? Science 295, 313–315.

Lin, J.-F., Campbell, A.J., Heinz, D.L., Shen, G., 2003a. Static compression of iron–silicon alloys: implications for silicon in the Earth's core. J. Geophys. Res. 108, 2045.

Lin, J.-F., Struzhkin, V.V., Sturhahn, W., Huang, E., Zhao, J., Hu, M.Y., Alp, E.E., Mao, H.-K., Boctor, N., Hemley, R.J., 2003b. Sound velocities of iron–nickel and iron–silicon alloys at high pressures. Geophys. Res. Lett. 30, 2112.

Lin, J.-F., Sturhahn, W., Zhao, J., Shen, G., Mao, H.-K., Hemley, R.J., 2005. Sound velocities of hot dense iron: Birch's law revisited. Science 308, 1892–1894.

Lin, J.-F., Scott, H.P., Fischer, R.A., Chang, Y.-Y., Kantor, I., Prakapenka, V.B., 2009. Phase relations of Fe–Si alloy in Earth's core. Geophys. Res. Lett. 36, L06306.

Lord, J.A.E., Beshers, D.N., 1965. Elastic stiffness coefficients of iron from 77° to 673°K. J. Appl. Phys. 36, 1620–1623.

Luo, W., Johansson, B., Eriksson, O., Arapan, S., Souvatzis, P., Katsnelson, M.I., Ahuja, R., 2010. Dynamical stability of body center cubic iron at the Earth's core conditions. Proc. Natl. Acad. Sci. U.S.A. 107, 9962–9964.

Machová, A., Kadečková, S., 1977. Elastic constants of iron–silicon alloy single crystals. Czech. J. Phys. B 27, 555–563.

Mainprice, D., Barruol, G., IsmaïL, W.B., 2000. The seismic anisotropy of the Earth's mantle: from single crystal to polycrystal. In: Karato, S. et al. (Eds.), Earth's Deep Interior: Mineral Physics and Tomography from the Atomic to the Global Scale, Geophysical Monograph Series, vol. 117. American Geophysical Union, Washington, DC, pp. 237–264.

Mao, H.-K., Bassett, W.A., Takahashi, T., 1967. Effect of pressure on crystal structure and lattice parameters of iron up to 300 kbar. J. Appl. Phys. 38, 272–276.

Mao, H.-K., Xu, J., Bell, P.M., 1986. Calibration of the Ruby pressure gauge to 800 kbar under quasi-hydrostatic conditions. J. Geophys. Res. 91, 4673–4676.

Mao, H.-K., Shu, J., Shen, G., Hemley, R.J., Li, B., Singh, A.K., 1998. Elasticity and rheology of iron above 220 GPa and the nature of the Earth's inner core. Nature 396, 741–743.

Mao, H.-K., Xu, J., Struzhkin, V.V., Shu, J., Hemley, R.J., Sturhahn, W., Hu, M.Y., Alp, E.E., Vočadlo, L., Alfè, D., Price, G.D., Gillan, M.J., Schwoerer-Böhning, M., Häusermann, D., Eng, P., Shen, G., Giefers, H., Lübbers, R., Wortmann, G., 2001. Phonon density of states of iron up to 153 gigapascals. Science 292, 914–916.

Mao, W.L., Sturhahn, W., Heinz, D.L., Mao, H.-K., Shu, J., Hemley, R.J., 2004. Nuclear resonant x-ray scattering of iron hydride at high pressure. Geophys. Res. Lett. 31, L15618.

Mao, Z., Lin, J.-F., Liu, J., Alatas, A., Gao, L., Zhao, J., Mao, H.-K., 2012. Sound velocities of Fe and Fe–Si alloy in the Earth's core. Proc. Natl. Acad. Sci. U.S.A. 109, 10239–10244.

Matsui, M., Anderson, O.L., 1997. The case for a body-centered cubic phase (α′) for iron at inner core conditions. Phys. Earth Planet. Inter. 103, 55–62.

Mattesini, M., Belonoshko, A.B., Buforn, E., Ramírez, M., Simak, S.I., Udías, A., Mao, H., Ahuja, R., 2010. Hemispherical anisotropic patterns of the Earth's inner core. Proc. Natl. Acad. Sci. U.S.A. 107, 9507–9512.

Mattesini, M., Belonoshko, A.B., Tkalcic, H., Buforn, E., Udias, A., Ahuja, R., 2013. Candy wrapper for the Earth's inner core. Sci. Rep. 3, 2096.

McDonough, W.F., Sun, S.s., 1995. The composition of the Earth. Chem. Geol. 120, 223–253.

McQueen, R.G., Fritz, J.N., Marsh, S.P., 1964. On the composition of the Earth's interior. J. Geophys. Res. 69, 2947–2966.

Mikhaylushkin, A.S., Simak, S.I., Dubrovinsky, L., Dubrovinskaia, N., Johansson, B., Abrikosov, I.A., 2007. Pure iron compressed and heated to extreme conditions. Phys. Rev. Lett. 99, 165505.

Murphy, C.A., Jackson, J.M., Sturhahn, W., 2013. Experimental constraints on the thermodynamics and sound velocities of hcp-Fe to core pressures. J. Geophys. Res. 118, 1999–2016.

Nguyen, J.H., Holmes, N.C., 2004. Melting of iron at the physical conditions of the Earth's core. Nature 427, 339–342.

Ohtani, E., Shibazaki, Y., Sakai, T., Mibe, K., Fukui, H., Kamada, S., Sakamaki, T., Seto, Y., Tsutsui, S., Baron, A.Q.R., 2013. Sound velocity of hexagonal close-packed iron up to core pressures. Geophys. Res. Lett. 40, 5089–5094.

Persson, J., Desgranges, C., Delhommelle, J., 2011. Polymorph selection during the crystallization of iron under the conditions of Earth's inner core. Chem. Phys. Lett. 511, 57–61.

Petrova, A.E., Krasnorussky, V.N., Stishov, S.M., 2010. Elastic properties of FeSi. J. Exp. Theor. Phys. 111, 427–430.

Poirier, J.-P., 1994. Light elements in the Earth's outer core: a critical review. Phys. Earth Planet. Inter. 85, 319–337.

Routbort, J.L., Reid, C.N., Fisher, E.S., Dever, D.J., 1971. High-temperature elastic constants and the phase stability of silicon–iron. Acta Metall. 19, 1307–1316.

Ruban, A.V., Belonoshko, A.B., Skorodumova, N.V., 2013. Impact of magnetism on Fe under Earth's core conditions. Phys. Rev. B 87, 014405.

Rubie, D.C., Nimmo, F., Melosh, H.J., 2007. Formation of the Earth's core. In: Stevenson, D.J. (Ed.), Treatise on Geophysics, Evolution of the Earth, vol. 9. Elsevier, Amsterdam, pp. 51–90.
Rubie, D.C., Frost, D.J., Mann, U., Asahara, Y., Nimmo, F., Tsuno, K., Kegler, P., Holzheid, A., Palme, H., 2011. Heterogeneous accretion, composition and core–mantle differentiation of the Earth. Earth Planet. Sci. Lett. 301, 31–42.
Sata, N., Ohfuji, H., Hirose, K., Kobayashi, H., Ohishi, Y., Hirao, N., 2008. New high-pressure B2 phase of FeS above 180 GPa. Am. Mineral. 93, 492–494.
Sha, X., Cohen, R.E., 2006. First-principles thermoelasticity of bcc iron under pressure. Phys. Rev. B 74, 214111.
Sha, X., Cohen, R.E., 2010. Elastic isotropy of ε-Fe under Earth's core conditions. Geophys. Res. Lett. 37, L10302.
Shankland, T.J., 1972. Velocity–density systematics: derivation from Debye theory and the effect of ionic size. J. Geophys. Res. 77, 3750–3758.
Shibazaki, Y., Ohtani, E., Fukui, H., Sakai, T., Kamada, S., Ishikawa, D., Tsutsui, S., Baron, A.Q.R., Nishitani, N., Hirao, N., Takemura, K., 2012. Sound velocity measurements in dhcp-FeH up to 70 GPa with inelastic X-ray scattering: implications for the composition of the Earth's core. Earth Planet. Sci. Lett. 313–314, 79–85.
Sinn, H., Alp, E.E., Alatas, A., Barraza, J., Bortel, G., Burkel, E., Shu, D., Sturhahn, W., Sutter, J.P., Toellner, T.S., Zhao, J., 2001. An inelastic X-ray spectrometer with 2.2 meV energy resolution. Nucl. Instrum. Methods Phys. Res. Sect. A 467–468, 1545–1548.
Sohl, F., Schubert, G., 2007. Interior structure, composition, and mineralogy of the terrestrial planets. In: Spohn, T. (Ed.), Treatise on geophysics, vol. 10. Elsevier, Amsterdam, pp. 27–68, Overview.
Steinle-Neumann, G., Stixrude, L., Cohen, R.E., Gülseren, O., 2001. Elasticity of iron at the temperature of the Earth's inner core. Nature 413, 57–60.
Steinle-Neumann, G., Cohen, R.E., Stixrude, L., 2004. Magnetism in iron as a function of pressure. J. Phys.: Condens. Matter 16, S1109.
Stixrude, L., Cohen, R.E., 1995. High-pressure elasticity of iron and anisotropy of Earth's inner core. Science 267, 1972–1975.
Stixrude, L., 2012. Structure of iron to 1 Gbar and 40,000 K. Phys. Rev. Lett. 108, 055505.
Tateno, S., Hirose, K., Ohishi, Y., Tatsumi, Y., 2010. The structure of iron in Earth's inner core. Science 330, 359–361.
Toellner, T.S., Alatas, A., Said, A.H., 2011. Six-reflection meV-monochromator for synchrotron radiation. J. Synchrotron Radiat. 18, 605–611.
Tsuchiya, T., Fujibuchi, M., 2009. Effects of Si on the elastic property of Fe at Earth's inner core pressures: first principles study. Phys. Earth Planet. Inter. 174, 212–219.
Vočadlo, L., Brodholt, J., Alfe, D., Price, G.D., Gillan, M.J., 1999. The structure of iron under the conditions of the Earth's inner core. Geophys. Res. Lett. 26, 1231–1234.
Vočadlo, L., Alfè, D., Gillan, M.J., Wood, I.G., Brodholt, J.P., Price, G.D., 2003. Possible thermal and chemical stabilization of body-centred-cubic iron in the Earth's core. Nature 424, 536–539.
Vočadlo, L., 2007. Ab initio calculations of the elasticity of iron and iron alloys at inner core conditions: evidence for a partially molten inner core? Earth Planet. Sci. Lett. 254, 227–232.
Vočadlo, L., Wood, I.G., Gillan, M.J., Brodholt, J., Dobson, D.P., Price, G.D., Alfè, D., 2008. The stability of bcc-Fe at high pressures and temperatures with respect to tetragonal strain. Phys. Earth Planet. Inter. 170, 52–59.
Vočadlo, L., Dobson, D.P., Wood, I.G., 2009. Ab initio calculations of the elasticity of hcp-Fe as a function of temperature at inner-core pressure. Earth Planet. Sci. Lett. 288, 534–538.
Wang, C.Y., 1970. Density and the constitution of the mantle. J. Geophys. Res. 75, 3264–3284.
Whitaker, M.L., Liu, W., Liu, Q., Wang, L., Li, B., 2009. Thermoelasticity of ε-FeSi to 8 GPa and 1273 K. Am. Mineral. 94, 1039–1044.
Zhang, J., Guyot, F., 1999. Thermal equation of state of iron and $Fe_{0.91}Si_{0.09}$. Phys. Chem. Miner. 26, 206–211.
Zhang, F., Oganov, A.R., 2010. Iron silicides at pressures of the Earth's inner core. Geophys. Res. Lett. 37, L02305.
Zhang, H., Punkkinen, M.P.J., Johansson, B., Hertzman, S., Vitos, L., 2010. Single-crystal elastic constants of ferromagnetic bcc Fe-based random alloys from first-principles theory. Phys. Rev. B 81, 184105.